VALIDATION OF A DOUBLE-LAYER BOUSSINESQ-TYPE MODEL FOR HIGHLY NONLINEAR AND DISPERSIVE WAVES

Florent Chazel[1], Michel Benoit[2] and Alexandre Ern[3]

A two-layer Boussinesq-type mathematical model has been recently introduced by the authors with the goal of modeling highly nonlinear and dispersive waves (Chazel et al. 2009). The analysis of this model has previously shown that it possesses excellent linear properties, up to kh = 10 at least, for dispersion, shoaling coefficient and vertical profile of orbital velocities. In the present work a numerical one-dimensional (1DH) version of model is developed based on a finite difference technique for meshing the spatial domain. It is then applied and verified against a set of three one-dimensional (1DH) test-cases for which either numerical or experimental reference results are available: i. nonlinear and dispersive regular waves of permanent form; ii. propagation of regular waves on a trapezoidal bar (laboratory experiments by Dingemans (1994)); iii. shoaling and propagation of irregular waves on a barred beach profile (laboratory experiments by Becq-Girard et al. (1999)). The test-cases considered in this study confirm the very good capabilities of the model to reproduce either exact solutions, high-precision numerical simulations and experimental measurements in a variety of non-breaking wave conditions and types of bottom profiles. Nonlinearity, dispersion and bathymetric effects are well accounted for by the model, which appears to possess a rather wide domain of validity while maintaining a reasonable level of complexity.

Keywords: wave; wave modeling, Boussinesq model; nonlinear waves; dispersive waves

INTRODUCTION

During the past two decades, Boussinesq-type models have emerged as an attractive and commonly used tool for coastal applications and engineering purposes. Historically, Boussinesq-type models are based on two fundamental assumptions, namely weak nonlinearity and weak dispersion (e.g. Peregrine, 1967), making their dispersion properties poor in intermediate depths, and limiting the largest wave height that can be accurately modeled. As a result, substantial efforts have been devoted to extend the linear and nonlinear range of applicability of Boussinesq-type models. First, Nwogu (1993) and Wei et al. (1995) efficiently removed the weak nonlinearity assumption, allowing the model to simulate wave propagation in intermediate depths with strong nonlinear interactions. Some years later, Gobbi et al. (2000), Agnon et al. (1999) and Madsen et al. (2002) successfully removed the intermediate depth limitation with so-called high-order Boussinesq-type models, whose range of applicability reaches deep water areas, but with a significant increase in computational cost mainly due to the use of high order derivatives.

With the aim of developing a model which is applicable to complex domains (such as coastal areas, islands or estuaries) and accurate up to deep water, but with lower complexity than the previous models (i.e. lower order of derivatives and lower number of equations), the author have recently derived a new Boussinesq-type model based on a double-layer approach (Chazel et al. 2009). Assuming the flow to be irrotational and the bottom slope to be mild, the problem is formulated in terms of the velocity potential, thereby lowering the number of unknowns. The model derivation combines two approaches, namely 1) the method proposed by Agnon et al. (1999) and enhanced by Madsen et al. (2002) which consists in constructing infinite-series Taylor solutions to the Laplace equation, truncating them at a finite order and using Padé approximants, and 2) the double-layer approach of Lynett & Liu (2004) allowing to lower the order of derivatives. The final model consists of only four equations both in one and two horizontal dimensions, and includes only second-order derivatives, which is a major improvement in comparison with so-called high-order Boussinesq models.

In the remainder of this paper, we propose a brief outline of the mathematical model. Then we present a set of three validation test-cases in one horizontal dimension (1DH) with both analytic and laboratory data to assess the nonlinear behavior in intermediate and deep water. We first consider the propagation of nonlinear and dispersive regular waves of permanent form. The second test is the classical set of experiments by Dingemans (1994) for the propagation of regular waves over an underwater trapezoidal bar. The third test corresponds to the propagation of non-breaking irregular

[1] Université de Toulouse, UPS/INSA, Institut de Mathématiques de Toulouse, CNRS UMR 5219, 135 avenue de Rangueil, 31077 Toulouse cedex 4, France

[2] Université Paris Est, Saint-Venant Laboratory for Hydraulics, 6 quai Watier, 78401 Chatou cedex, France

[3] Université Paris-Est, CERMICS, Ecole des Ponts ParisTech, 6-8 avenue Blaise Pascal Cité Descartes, Champs-sur-Marne, 77455 Marne-La-Vallée cedex 2, France

waves over a barred profile by simulating flume experiments by Becq-Girard et al. (1999). This last test case allows to examine the behavior of the model to represent the evolution of the wave spectrum along the beach profile, with particular attention paid to the growth and decay of super-harmonic peaks as waves propagate towards the coastline.

BRIEF DESCRIPTION OF THE MATHEMATICAL MODEL

We consider the evolution of an inviscid and incompressible fluid with a free surface under the only influence of gravity. The flow is assumed to be irrotational, and the capillary effects owing to the presence of surface tension are neglected. Moreover, we assume constant atmospheric pressure at the free surface of the fluid. The time-dependent fluid domain is bounded from below by a static sea bottom, defined by $z = \bar{z}(X) = -h(X)$, and from above by a time-dependent free surface, denoted by $z = \eta(t, X)$. The level $z = 0$ corresponds to the still-water level. As shown in Fig. 1, the fluid is divided into two layers by an interface $z = \hat{z}(X) = -\sigma h(X)$, where σ is an arbitrary parameter to be chosen in the range]0 ; 1[. We point out that this division of the fluid domain into two layers is purely conceptual since both layers have the same density. As far as the bathymetry is concerned, we assume that the still-water depth h verifies $|\nabla h| << 1$, which corresponds to the classical mild-slope approximation.

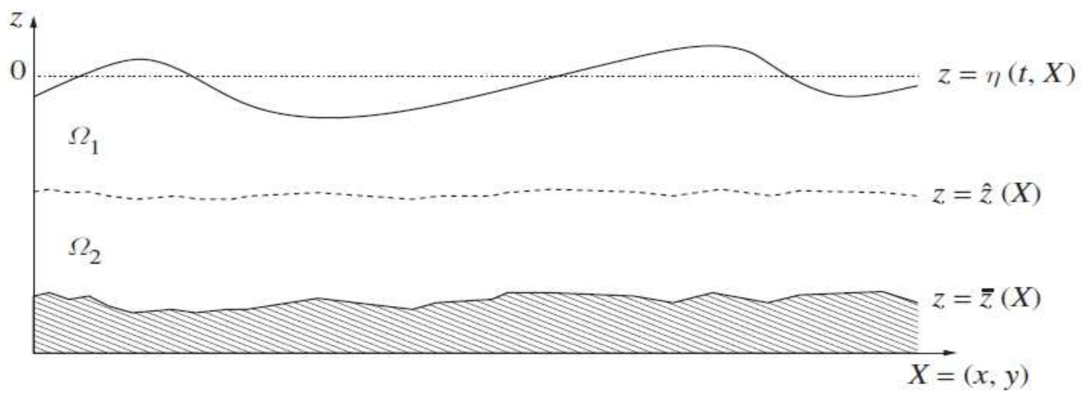

Figure 1. Representation of the fluid domain with a two-layer approach.

Since the flow is assumed irrotational, the problem can be formulated in terms of the velocity potential $\phi(t, X, z)$ of the fluid, along with the free surface $\eta(t, X)$, thus lowering the number of unknowns. The fluid motion is then governed by ten equations: one Laplace equation for each layer, one Bernoulli equation at the surface of each layer, three continuity conditions at the interface between the layers on the potential ϕ, the vertical velocity w and the pressure p, two boundary conditions expressing that the free surface and the bottom are bounding surfaces, and a condition on the pressure at the free surface. Following Zakharov (1968), this three-dimensional problem can be rewritten as a two-dimensional problem by projecting the equations on the free surface and introducing a classical Dirichlet-Neumann Operator (DNO) $\mathcal{G}[\eta, h]$, such that:

$$\tilde{w}_1 = \mathcal{G}[\eta, h]\tilde{\phi}_1 \tag{1}$$

where $\tilde{\phi}_1(t, X) = \phi_1(t, X, z = \eta(t, X))$ is the velocity potential at the free surface and $\tilde{w}_1(t, X) = w_1(t, X, z = \eta(t, X))$ is the vertical velocity at the surface. This equivalent problem then only consists in three equations on the potential at the surface, the vertical velocity at the surface, and the free surface elevation $\eta(t, X)$, where the double-layer modeling is concentrated in the DNO $\mathcal{G}[\eta, h]$.

The main difficulty in finding an approximation to this Dirichlet-Neumann operator is that it involves solving the Laplace equations along with the boundary and continuity conditions on a time-dependent domain. An interesting work-around to this issue consists in constructing an alternative Dirichlet-Neumann operator expressed at the still-water level called $\mathcal{G}_0[h] = \mathcal{G}[0, h]$, and then finding a closure between the unknowns at the free surface and the ones at the still-water level $z = 0$. These closure relations are easily obtained via truncated Taylor expansions of the potential and the vertical velocity between the free surface and the still-water level $z = 0$, where the truncation orders can be motivated by a dimensional analysis. An intermediate model –consisting of four equations– is then obtained by including these two closure relations into the Zakharov formulation. The main advantage of this reformulation is that the translated Dirichlet-Neumann operator $\mathcal{G}_0[h]$ is static, and can thus be computed once and for all at $t = 0$.

The last step in the model derivation is to construct an approximation of the static Dirichlet-Neumann operator $\mathcal{G}_0[h]$. To this end, we follow the generalized Boussinesq procedure introduced by Madsen et al. (2002, 2003) which consists in looking for a solution of the Laplace equation in each layer under the form of an infinite Taylor series in the vertical coordinate. These series are then truncated by retaining only the first two terms, this choice being again motivated by a careful dimensional analysis. In the last step, we introduce Padé approximants in order to lower the order of the derivatives in the truncated series. Finally, we obtain an expression of an approximate static Dirichlet-Neumann operator $\mathcal{G}_0^{\text{app}}[h]$ which only involves second-order spatial derivatives.

The final model reads as follows:

$$\left.\begin{array}{c} \partial_t\widetilde{\phi}_1 + \dfrac{1}{2}|\nabla\widetilde{\phi}_1|^2 - \dfrac{1}{2}\widetilde{w}_1{}^2(1+|\nabla\eta|^2) + g\eta = 0, \\ \partial_t\eta + \nabla\eta\cdot\nabla\widetilde{\phi}_1 - \widetilde{w}_1(1+|\nabla\eta|^2) = 0, \\ \left(1 - \dfrac{\eta^2}{2}\Delta + (\eta - \dfrac{\eta^3}{6}\Delta)\mathcal{G}_0^{\text{app}}[h]\right)\phi_0 = \widetilde{\phi}_1, \\ \widetilde{w}_1 = \left(-\eta\Delta + \left(1 - \dfrac{\eta^2}{2}\Delta\right)\mathcal{G}_0^{\text{app}}[h]\right)\phi_0, \end{array}\right\} \qquad (2)$$

where it is recalled that $\widetilde{\phi}_1(t,X)$ denotes the velocity potential at the free surface, $\widetilde{w}_1(t,X)$ denotes the vertical velocity at the free surface. ϕ_0 corresponds to the velocity potential at the still water level $z = 0$. The complete expression of $\mathcal{G}_0^{\text{app}}[h]$ is omitted here for brevity (see Chazel et al. (2009)).

A detailed analysis of the linear properties of the model (namely phase and group velocities, vertical profiles of both velocity potential and vertical velocity, the linear shoaling gradient) has been performed in Chazel et al. (2009). With the optimal value $\sigma = 0.314$, the previous model exhibits excellent dispersive properties, up to deep water.

NUMERICAL MODEL FOR SIMULATING ON-DIMENSIONAL (1DH) CASES

A one-dimensional (1DH) numerical model has been developed based on the SCILAB® software (http://www.scilab.org/) to solve eq. (2). The spatial domain is discretized with a constant mesh size, and all derivative operators in eq. (2) and in the expression of $\mathcal{G}_0^{\text{app}}[h]$ are approximated by centred finite difference formulas over a 5-point stencil. This yields fourth-order accuracy in space for both 1st-order and 2nd-order derivatives.

Time integration is performed with the standard fourth-order four-stage explicit Runge–Kutta scheme with constant time-step. This scheme is known to possess a wide stability region. However, owing to the nonlinear nature of the considered test-cases, this scheme can develop some high-frequency instabilities for some cases. To avoid such instabilities, a 8th-order Savitzky–Golay smoothing filter is applied after each time step to η, $\widetilde{\phi}_1$ and $\widetilde{w}_1$. It was checked that the use of this filter introduces a negligible loss of accuracy of the model.

In order to simulate the behavior of a wave tank, relaxation zones are used at both ends of the domain. These zones can be used either to generate incident –regular or irregular– waves or to absorb outgoing waves. We refer to e.g. Bingham and Agnon (2005) for more details on this method. Finally, Neumann and periodic conditions are easily imposed by reflecting, respectively evenly and periodically, coefficients corresponding to points located outside the domain, thus making the discretization of the differential operators very regular.

VALIDATION TEST-CASES

The numerical model is applied on three different cases for which either numerical or experimental reference data is available. These applications are described in the following three sub-sections. All computations have been performed with the deep-water (kh = 10) optimal value σ = 0.314.

Stable and periodic nonlinear dispersive waves over a flat bottom

The first test-case concerns the propagation over a flat bottom of nonlinear and dispersive periodic waves of permanent shape. For this situation reference solutions can be obtained by the so-called Stream Function Method (e.g. Dean 1965; Rienecker and Fenton 1981), which is a numerical method with very high accuracy for such periodic and stable waves.

We choose here the following parameters for the waves: a wave length L = 64 m and a wave height H = 6.4 m, with a water depth h = 96 m. There is no Eulerian ambient current in the simulation. Based on these values the measure of wave nonlinearity (steepness) is $\varepsilon = H/L$ = 10%, or alternatively $kH/2 = \pi/10 \approx 0.31$, which represents a quite strong nonlinear case. The measure of dispersion is $\mu = kh = 3\pi$ or alternatively h/L = 1.5, which is well above the limit traditionally considered for deep water ($\mu = \pi$ or h/L = 0.5). Those conditions are thus very demanding for Boussinesq-type models.The computational domain covers one wave-length and comprises 32 nodes (Δx = 2 m). Periodic boundary conditions are used on this case to model the propagation of the considered wave over a distance of several wave-lengths. The time-step is chosen as T/50, where T = 6.094 s, is the wave period as computed by the Stream Function method. Initial conditions of the simulation are provided by a 20[th]-order Stream Function solution, provided by the code Stream_HT (Benoit et al. 2002). This solution is also used afterwards as reference to compare with the results of the numerical model after several periods of wave propagation.

Results for the free surface elevation and free surface potential at times t = 10T and t = 25T are presented on Fig. 2 and 3 respectively.

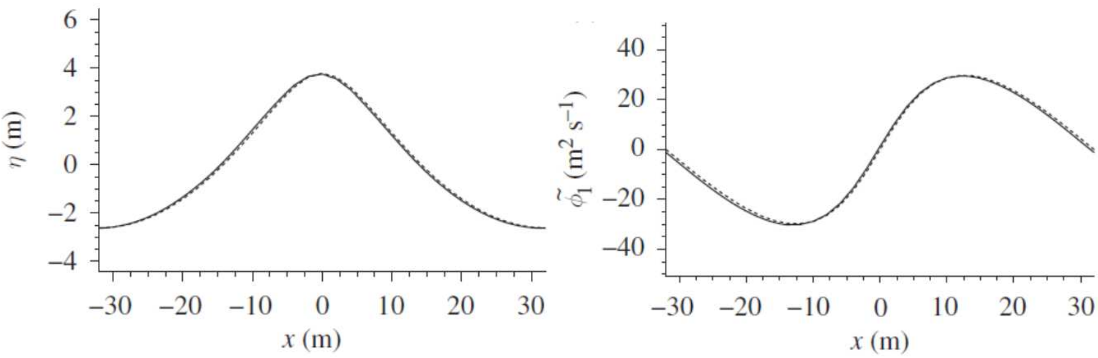

Figure 2. Snapshots of the free surface elevation (left panel) and free surface velocity potential (right panel) at time *t* = 10*T*. The solid line is the present model with σ = 0.314 and the dotted line is the stream function reference solution.

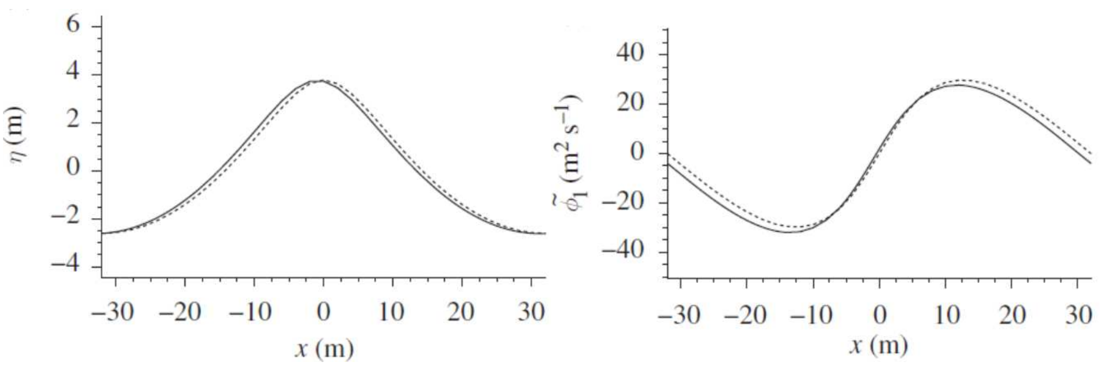

Figure 3. Same as Figure 2, but at time *t* = 25*T*.

Comparison of model's results with the reference solution shows extremely good agreement up to time $t \approx 20T$, after which small discrepancies become observable. Other runs on this case have been performed by increasing the number of nodes from 32 up to 128 in order to check the grid convergence. Based on this analysis, the difference observed on Fig. 3 can be attributed to the approximation in the numerical model, where 4^{th}-order (and higher) nonlinear terms have been neglected in the final formulation of the model. However, it is observed that the agreement with the reference solution is still good at $t = 25T$. The shapes of the waves are the same, and their amplitudes are equal; only a small phase shift with the reference solution is observed. Comparing the computed and theoretical positions of the wave crests at $t = 25T$ we can evaluate the nonlinear phase celerity error, which is here 0.08 % approximately, bringing confirmation of the excellent capability of the model to handle such dispersive ($kh = 3\pi \approx 10$) and nonlinear ($H/L = 10\%$) waves.

Regular waves over a submerged bar (Dingemans experiment, 1994)

The model is then applied to the propagation of regular waves over a submerged trapezoidal bar by considering the wave flume experiments performed by Dingemans (1994), which often serve as reference cases for testing nonlinear wave models. In this situation, both nonlinear and dispersion effects are important. Nonlinear interactions lead to the development of higher harmonic components in the wave train, which are released over the mound of the bar and then propagate as free waves after the bar. Accurate dispersion modeling is thus needed to represent this decomposition of the incident wave train. The bottom profile in the wave flume is presented on Fig. 4, together with the locations of the 11 waves probes where time-series of free surface elevations were recorded. We model here two of the test-cases performed by Dingemans (1994), namely case A (incident wave parameters : H = 2.0 cm and T = 2.02 s) and case C (H = 4.1 cm and T = 1.01 s).

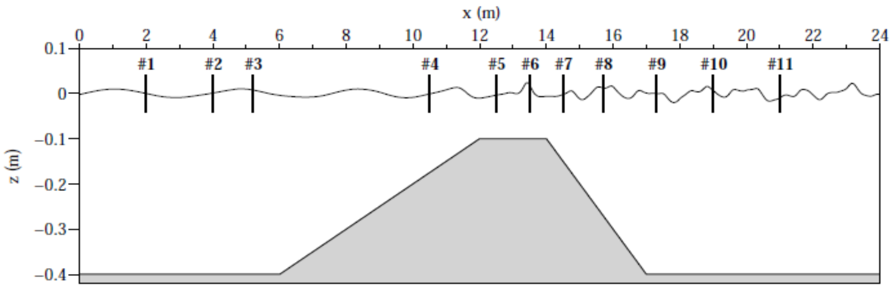

Figure 4. Bottom profile and position of wave gauges for the wave flume experiments of Dingemans (1994).

Time-series of free surface elevation computed by the model are compared to experimental measurements at stations 8 to 11, which are all located after the bar. It is known that the signals at these probes are the most difficult to reproduce by numerical models, due to dispersive effects which are more pronounced for the super-harmonics released after the bar.

Results of case A (H = 2.0 cm ; T = 2.02 s) are presented on Fig. 5. For this case the incident waves are rather long (kh = 0.67 offshore of the bar) and thus weakly dispersive, and have a low steepness ($kH/2$ = 0.017 or H/L=0.0053). The transformation of this incident regular and quasi-sinusoidal wave train into a series of free waves which propagate at their own celerity is clearly visible on Fig. 5, as the wave profiles are very different from one station to another. After the bar high-order harmonic components mainly evolve as free waves whereas they remained bounded to the main wave component during the shoaling of wave on the offshore slope of the bar. The various panels of Fig. 5 show that almost all the details of the wave profiles are reproduced by the simulations indicating that both the amplitudes and celerities of the released super-harmonics are properly modeled.

Results of case C (H = 4.1 cm ; T = 1.01 s) are presented on Fig. 6. For this case the incident waves are shorter (kh = 1.69 offshore of the bar) and thus more dispersive, and also steeper ($kH/2$ = 0.087 or H/L=0.028). Although the comparison of model's results with measurements is not as good as for case A, it is still of very high quality. The shapes of the waves at the four stations are very well reproduced by the model. Only the amplitudes of modeled waves may appear somewhat overestimated at stations 10 and 11, but on can also note the measured waves are not fully repetitive on the figure. On this case the proportion of energy transferred from the main components to super-harmonic components is lower in comparison to the former case, leading to a more homogeneous and regular wave field after the bar.

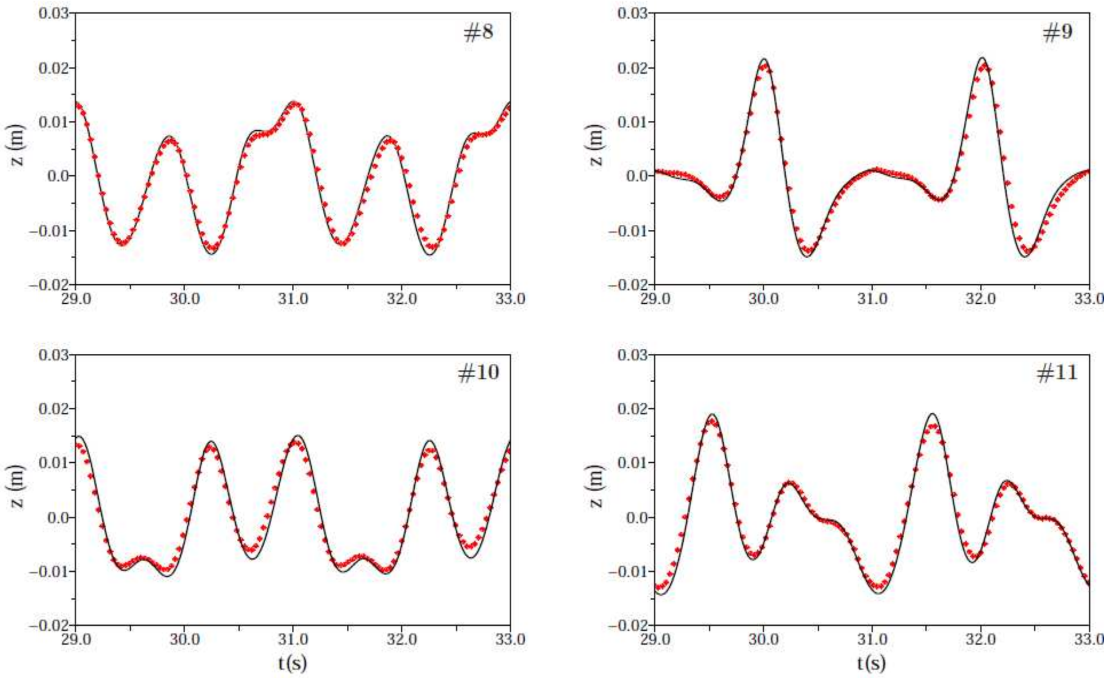

Figure 5. Time-series of free surface elevation at the four gauges located after the bar (gauges 8 to 11) for case C of Dingemans (1994) (*H* = 2.0 cm ; *T* = 2.02 s). Black line: results of the present numerical model ; red dots: measurements in the wave flume.

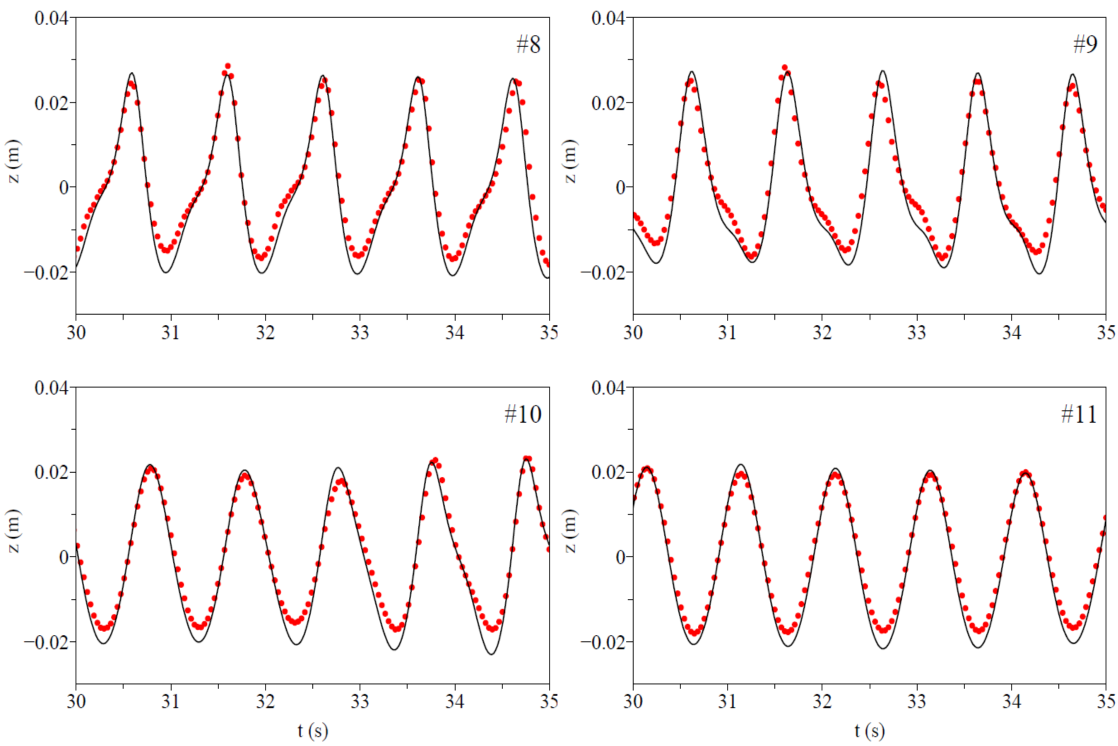

Figure 6. Time-series of free surface elevation at the four gauges located after the bar (gauges 8 to 11) for case C of Dingemans (1994) (*H* = 4.1 cm ; *T* = 1.01 s). Black line: results of the present numerical model ; red dots: measurements in the wave flume.

Random waves over a barred beach (Becq-Girard et al. (1999) experiment)

As a final test we consider non-breaking irregular wave conditions over a barred bottom profile. Becq-Girard et al. (1999) performed a series of experiments in a wave flume at EDF R&D LNHE in Chatou (France). The flume is 45 m long and 0.60 m wide. It is equipped with a piston-type wave-maker which can generate either monochromatic waves or irregular sea states corresponding to a specified variance spectrum (e.g. of JONSWAP-type). The bottom profile (cf. Fig. 7) represents a submerged bar over which nonlinear effects affect the dynamics of wave propagation in a significant manner. The bottom profile was made of smooth metal sheets and an absorbing sponge layer was set up in the upper part of the beach so that bottom friction dissipation and reflection from the beach can be regarded as negligible in the experiments.

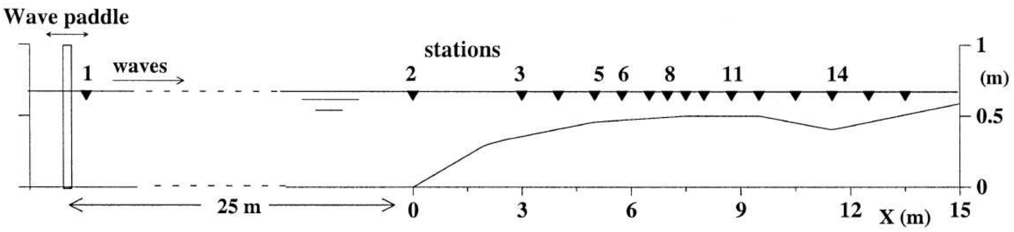

Figure 7. Lay-out of the set-up for the irregular flume experiments by Becq-Girard et al. (1999).

For the test-case considered here (test 26) the water depth offshore of the bathymetric profile is 0.65 m. It decreases down to 0.15 m in the shallowest part of the bar. This case corresponds to non-breaking conditions. At the beginning of the bottom slope (probe 2 at x = 0) the measured spectral significant wave height is H_{mo} = 0.034 m and the peak frequency is f_p = 0.4185 Hz (peak period T_p = 2.39 s). The simulated wave spectrum is of JONSWAP-type with a peak enhancement factor γ = 3.3. The measured spectrum at probe 2 is plotted on Fig. 8.

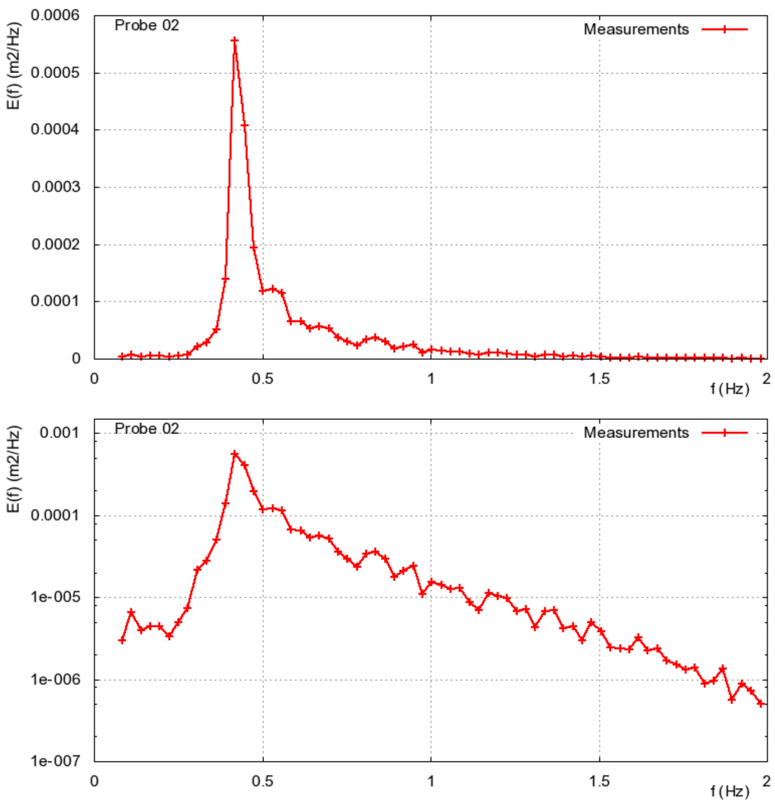

Figure 8. Variance spectrum measured at probe 2 for test 26 of Becq-Girard et al. (1999). Note that linear (logarithmic) scale is used for spectral density (vertical axis) on the upper (lower) plot.

A series of 16 resistive-type wave probes were deployed along the bathymetric profile (cf. Fig. 7). Free surface elevation time series were recorded over a duration of 40 minutes (corresponding of about 1000 waves of period T_p) with a sampling time-step of 0.070 s (corresponding to about 34 points per wave of period T_p).

A computational mesh of length 25 m (covering the range [-5 m; 20 m] on Fig. 7) is constructed with a mesh size of Δx = 0.1 m (250 nodes). This corresponds to about 65 points per peak wave length over the offshore part of the domain. The time step is Δt = 0.0657 s, which is T_p/35. The numerical simulation covers approximately the same duration as the experimental records, namely 2 390 s (≈ 40 min) = 1000 T_p = 35 000 Δt. The time-series of free surface elevation at probe 2 is issued as boundary condition to drive the numerical simulation, so that the measured and simulated spectra at probe 2 are the same (see Fig. 8).

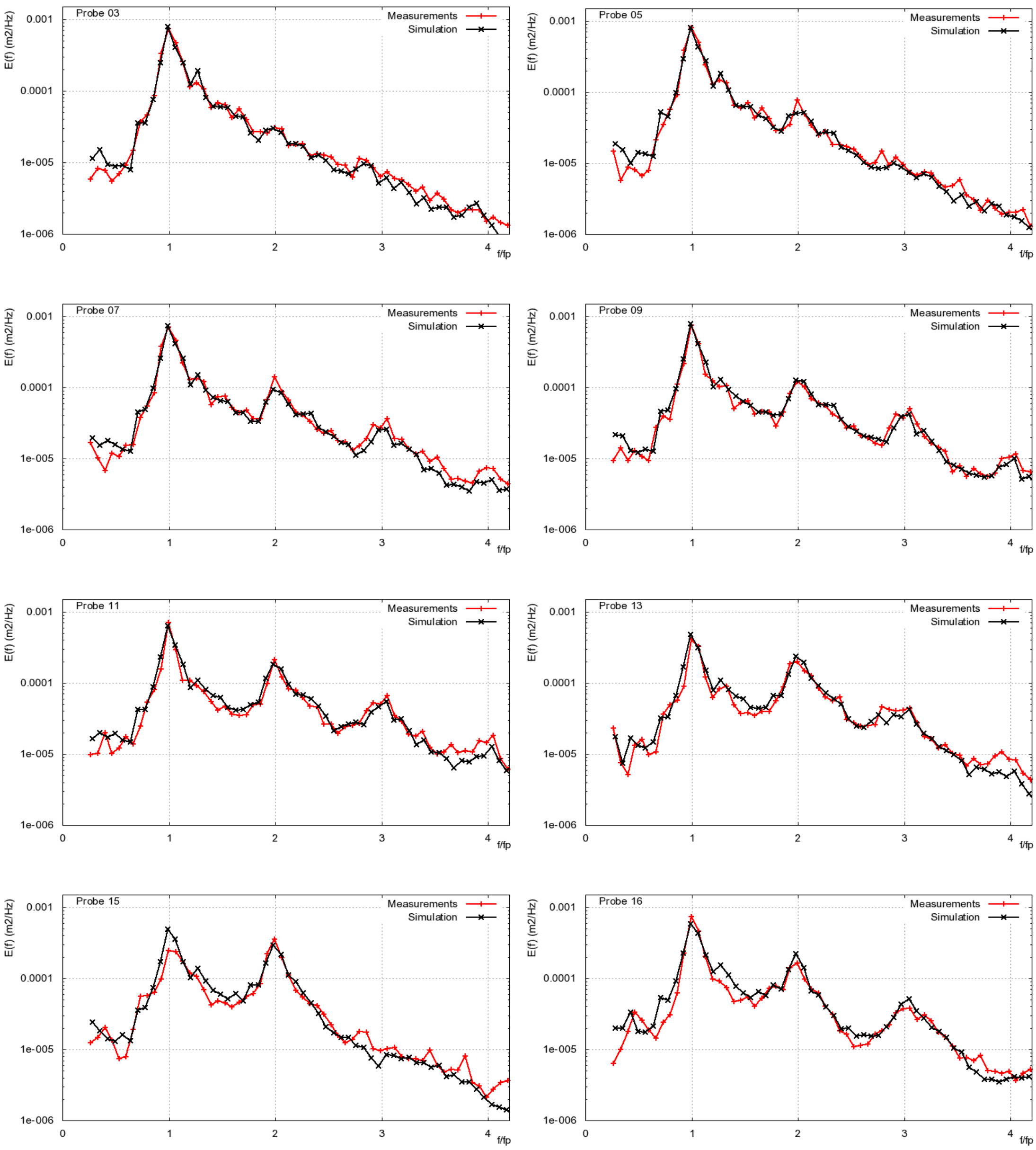

Figure 9. Evolution of frequency variance spectrum along the bathymetric profile (at probes 3, 5, 7, 9, 11, 13 15 and 16) for test 26 of Becq-Girard et al. (1999). Measured spectra are in red with + symbols; model spectra are in black with x symbols. Logarithmic scale is used for spectral density (vertical axis).

From the simulated time-series variance spectra $E(f)$ are computed by a spectral analysis software based of the so-called periodogram method, and compared with measured spectra computed using the same technique. The variance spectra at probes 3, 5, 7, 9, 11, 13, 15 and 16 are plotted on Fig. 9. On this figure the frequencies are normalized by the peak frequency (so as to let appear in clear way the super-harmonics components at frequencies $2f_p$, $3f_p$, etc.). Note also that a logarithmic scale is used for the spectral density (vertical axis). This sequence of spectra clearly shows the transfer of energy from the main peak to higher harmonics as the water depth decreases, first towards the $2f_p$ harmonic (probes 3 and 5), then towards the $3f_p$ harmonic (probe 7) and eventually towards the $4f_p$ harmonic (probes 9 and 11). The development of these super-harmonics peaks is very well reproduced by the model with the correct amplitudes for each of these peaks. As the water increases after the shoal (probes 13 and 15), we observe that the amplitudes of the $4f_p$ and then $3f_p$ harmonics are significantly reduced in very good agreement with the measured spectra. Eventually at station 16 where the water depth is decreasing again shoaling and nonlinear effects manifest again and the $3f_p$ harmonic starts again gaining energy, a trend also fully given by the model.

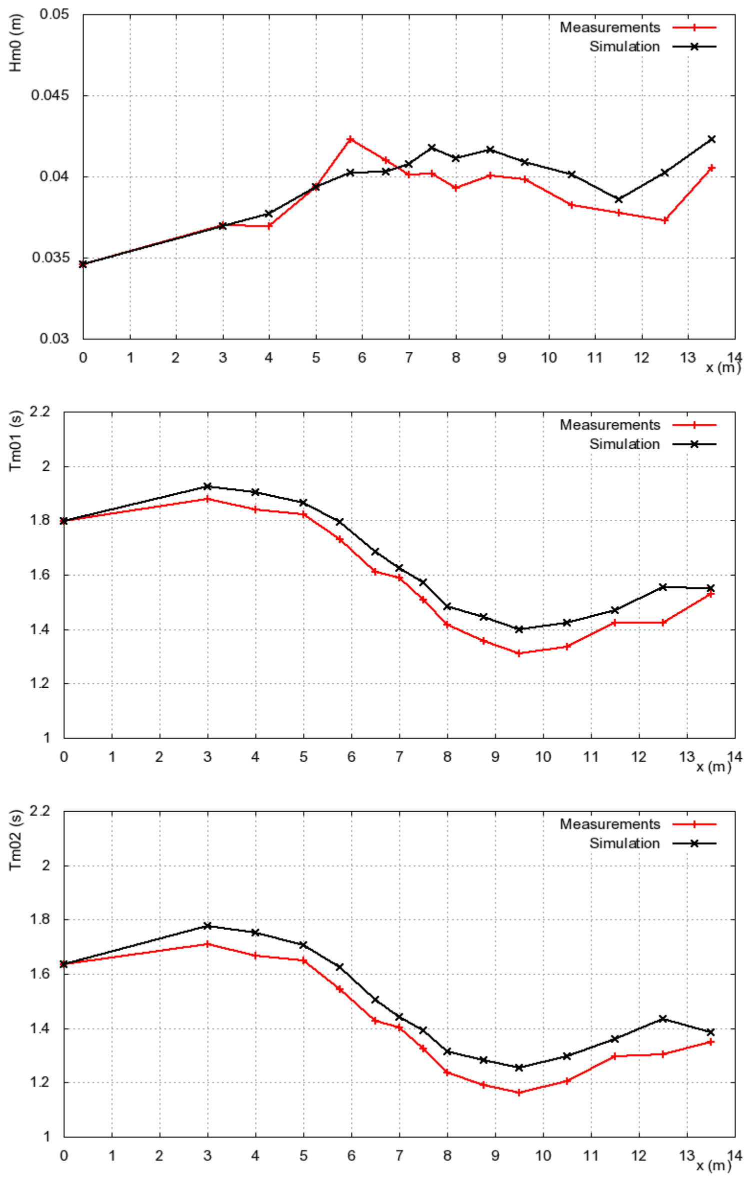

Figure 10. Evolution of integrated spectral wave parameters along the bathymetric profile for test 26 of Becq-Girard et al. (1999). Upper plot: significant wave height H_{mo}; middle plot: mean period T_{m01}; lower plot: mean period T_{m02}. Parameters computed from measured spectra are in red with + symbols; parameters computed from model spectra are in black with x symbols.

From the variance spectra a number of characteristic wave parameters can be computed. We plot on Fig. 10 the evolution along the bathymetric profile the spectral significant wave height $H_{m0} = 4\sqrt{m_0}$, and the mean periods $T_{m01} = m_0 / m_1$ and $T_{m02} = \sqrt{m_0 / m_2}$ computed from the spectral moments m_n, defined by:

$$m_n = \int_{f_{\min}}^{f_{\max}} f^n E(f) df \tag{3}$$

For these three parameters the general trends of evolution are well simulated by the model but with a small overestimation both for wave height and mean periods. In particular the decrease of the mean periods as the water depth decreases (i.e. between x = 3 m and 9 m) as a consequence of the transfer of energy towards super-harmonics is properly modeled, and so is the slight increase of these mean periods after the shoal where the water depth is greater.

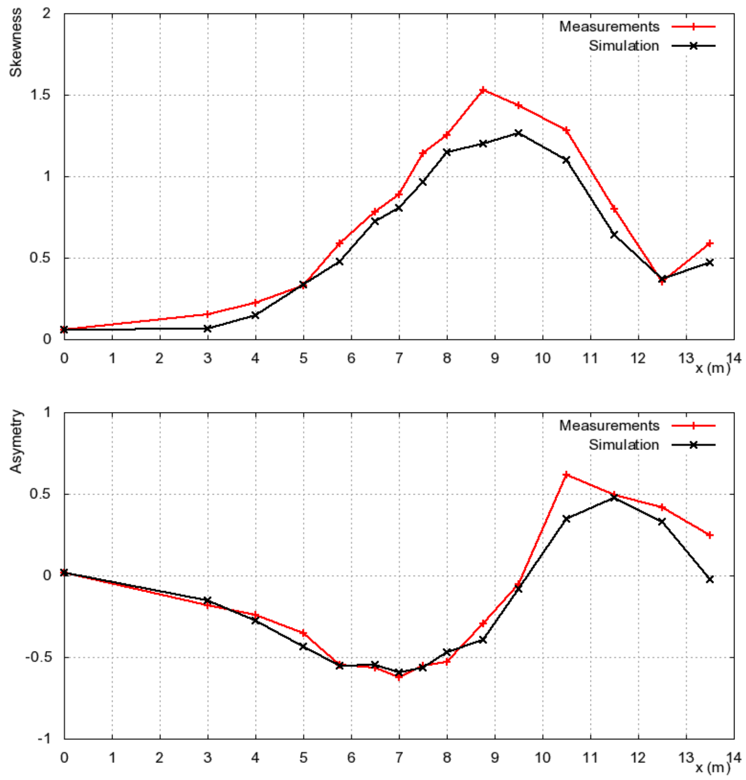

Figure 11. Evolution of nonlinear wave parameters along the bathymetric profile for test 26 of Becq-Girard et al. (1999). Upper plot: skewness (horizontal asymmetry) λ_3; lower plot: vertical asymmetry *A*. Parameters computed from measured bi-spectra are in red with + symbols; parameters computed from model bi-spectra are in black with x symbols.

Finally, in order to characterize the nonlinear effects, we compute and plot on Fig. 11 two parameters, namely the skewness λ_3 and the vertical asymmetry A, respectively defined by:

$$\lambda_3 = \frac{\left\langle \left(\eta - \langle \eta \rangle\right)^3 \right\rangle}{m_o^{3/2}} = \frac{\sum_{m=-\infty}^{+\infty} \sum_{n=-\infty}^{+\infty} \mathrm{Re}\left[B_{m,n}\right]}{m_o^{3/2}} \tag{4}$$

$$A = \frac{\sum_{m=-\infty}^{+\infty} \sum_{n=-\infty}^{+\infty} \mathrm{Im}\left[B_{m,n}\right]}{m_o^{3/2}} \tag{5}$$

where $B_{m,n} = B(f_m, f_n)$ is the bispectrum, defined as the Fourier transform of the third-order correlation function of the surface elevation. The bispectrum can be used to identify coupled modes in the wave train (see *e.g.* Kim and Powers 1979; Kim et al. 1980; Elgar and Guza 1985; Becq-Girard et al. 1999).

The skewness λ_3 is a measure of the horizontal asymmetry of the waves. As the wave shoals on the bottom profile (i.e. for x = 0 to 9 m) we can clearly see an increase of this parameter, from almost 0 to about 1.5 for the measurements and 1.3 for the model. Then the skewness decreases between x = 9.5 and 12.5 m when the water depth increases after the shoal, and eventually it increases at probe 16 as water depth is decreasing again. These trends are well reproduced by the model although the model's values are in general a bit lower than the measured ones.

The vertical asymmetry A of the wave signal can be obtained by integrating the imaginary part of the bispectrum (Masudo and Kuo 1981). The lower panel of Fig. 11 shows that the evolution of the vertical asymmetry is modeled with great accuracy. First it decreases from A = 0 to –0.6 for x ranging from 0 to about 7 m, then it increases up to about 0.5-0.6 for x ranging from 7 m to about 11 m, then it decreases again as the waves shoal on the last slope of the profile.

SUMMARY OF THE STUDY AND OUTLOOK

The new model recently proposed by Chazel et al. (2009) exhibits a number of advantages. Firstly, a property shared by other Boussinesq-type models, we recall that it is a 2DH model, making it clearly less heavy to use than a full 3D hydrodynamical model. Secondly, due to the use of a potential formulation the model involves only 4 equations to solve, both for 1DH and 2DH cases. Thirdly, only first and second order space derivatives appear in model equations, which greatly simplifies the numerical implementation compared to other high-order Boussinesq-type models that involve up to fifth order derivatives. Fourthly, we have proposed the use of a static Dirichlet-to-Neumann operator (DNO), which has to be computed once for all at the beginning of the simulation, saving thus a large amount of CPU time.

Analysis of model's properties has revealed that it possesses excellent linear characteristics, up to kh = 10 at least, for dispersion, shoaling coefficient and vertical profile of velocity. The three 1DH test-cases considered in this study have shown very good capabilities of the model to reproduce exact numerical solutions and experimental measurements in a variety of non-breaking wave conditions and types of bottom profiles. Nonlinearity, dispersion and bathymetric effects are well reproduced by the model, which appears to possess a rather wide domain of validity while having a reasonable level of complexity.

Ongoing and future work will address a number of improvements of this model, namely its extension to deal with 2DH cases (with the aim of using unstructured meshes for the coastal domain of interest), the modeling of dissipative processes (namely bottom friction dissipation and depth-induced breaking), the appropriate numerical representation of various types of coastal/harbor structures in the model, and the modeling of run-up and run-down of wave on slopes.

REFERENCES

Agnon, Y., P.A. Madsen, and H.A. Schäffer. 1999. A new approach to high-order Boussinesq models. *Journal of Fluid Mechanics*, 399, 319–333.

Becq-Girard, F., P. Forget, and M. Benoit. 1999. Non-linear propagation of unidirectional wave fields over varying topography. *Coastal Engineering*, 38, 91–113.

Benoit, M., M. Luck, C. Chevalier, and M. Bélorgey. 2002. Near-bottom kinematics of shoaling and breaking waves: experimental investigation and numerical prediction. *Proceedings of 28th International Conference on Coastal Engineering* (Cardiff, UK), 306–318. ed. J. McKee Smith, World Scientific.

Bingham, H.B., and Y. Agnon. 2005. A Fourier–Boussinesq method for nonlinear water waves. *European Journal of Mechanics. B/Fluids*, 24, 255–274.

Chazel, F., M. Benoit, A. Ern, and S. Piperno. 2009. A double-layer Boussinesq-type model for highly nonlinear and dispersive waves. *Proceedings of the Royal Society of London*, A 465, 2319–2346.

Dean, R.G. 1965. Stream function representation of nonlinear ocean waves. *Journal of Geophysical Research*, 70, 4561–4572.

Dingemans, M. 1994. Comparison of computations with Boussinesq-like models and laboratory measurements. *Mast-G8M technical report H1684*. Delft Hydraulics, Delft, The Netherlands.

Elgar, S., and R.T. Guza. 1985. Observations of bispectra of shoaling surface gravity waves. *Journal of Fluid Mechanics*, 161, 425–448.

Gobbi, M.F., J.T. Kirby, and G. Wei. 2000. A fully nonlinear Boussinesq model for surface waves. Part 2. Extension to $O((kh)^4)$. *Journal of Fluid Mechanics*, 405, 181–210.

Kim, Y.C., and E.J. Powers. 1979. Digital bispectral analysis and its application to the non-linear wave interactions. *IEEE Transactions on Plasma Science*, 7(2), 120–131.

Kim, Y.C., J.M. Beall, E.J. Powers, and R.W. Miksad. 1980. Bispectrum and nonlinear wave coupling. *Physics of Fluids*, 23(2), 258–263.

Lynett, P., and P.L.F. Liu. 2004. A two-layer approach to wave modeling. *Proceedings of the Royal Society of London*, A 460, 2637–2669.

Madsen, P.A., H.B. Bingham, and H. Liu. 2002. A new Boussinesq method for fully nonlinear waves from shallow to deep water. *Journal of Fluid Mechanics*, 462, 1–30.

Madsen, P.A., H.B. Bingham, and H.A. Schäffer. 2003. Boussinesq-type formulations for fully nonlinear and extremely dispersive water waves: derivation and analysis. *Proceedings of the Royal Society of London, Series A,* 459, 1075–1104.

Masudo, A., and Y.Y. Kuo. 1981. A note on the imaginary part of bispectra. *Deep Sea Research*, 28A, (3), 213–222

Nwogu, O.G. 1993. An alternative form of the Boussinesq equations for nearshore wave propagation. *Journal of Waterway, Port, Coastal and Ocean Engineering*, 119(6), 618–638.

Peregrine, D.H. 1967. Long waves on a beach. *Journal of Fluid Mechanics*, 27, 815–827.

Rienecker, M.M., and J.D. Fenton. 1981 A Fourier approximation for steady water waves. *Journal of Fluid Mechanics,* 104, 119–137.

Wei, G., J.T. Kirby, S.T. Grilli, and R. Subramanya. 1995. A fully nonlinear Boussinesq model for surface waves: Part I. Highly nonlinear unsteady waves. *Journal of Fluid Mechanics,* 294, 71–92.

Zakharov, V. E. 1968. Stability of periodic waves of finite amplitude on the surface of a deep fluid. *Journal of Applied Mechanics and Technical Physics,* 9, 190–194.